

# Review Article: The Chicken and Egg Problem in Pancreatic Ductal Adenocarcinoma

Rishabh Datta, Lohyun Kim, Florian Koehler, Yong-Chul Yoon

June 22, 2021

## BACKGROUND

Pancreatic ductal adenocarcinoma (PDA) is the most prevalent neoplastic disease of the pancreas, which accounts for more than 90% of all pancreatic diseases [1]. PDA is notorious for its low five-year survival rate, averaging approximately 6% [2]. The incidence of the disease in the U.S. and Europe is forecast to double in the next decade with corresponding increase in the number of death [3]. The principal reason, besides genetic predispositions, for this daunting prediction is the increase in the number of type II diabetics, a risk-factor for PDA. This is exacerbated by certain life-style habits, including alcohol and tobacco abuse.

The difficulty of treating PDA is attributed to its unique tumor microenvironment (TMIE). It is hypovascular, unlike many other tumors, hypoxic, and desmoplastic. The desmoplasia causes increased concentration of fibroblasts, immune cells and an excessive production of complex extracellular matrix (ECM), comprised of a dense network of collagen, proteoglycans and glycosaminoglycans (GAGs). In particular, the concentration of a particular GAG - hyaluronic acid (HA) - is typically much higher in PDA than in healthy pancreatic tissues. Desmoplasia and hypoxia in combination accumulates myeloid cells and macrophages that adopt an immunosuppressive, pro-angiogenic state [4] [5]. Hypovascularity is characterized not only by fewer blood vessels, but also with a relatively high number of collapsed vessels. The transport of small molecules which are delivered into the tumor is further inhibited by constraints on diffusion (caused by dense fibrotic ECM) and convection [6].

Currently, surgical resection followed by chemotherapy is the only curative therapy available. However, only about 15% of PDA patients can undergo this procedure as not all of the tumor

is resectable. For the remaining 85% of the patient, a systematic radiochemotherapy is the only available treatment option. Yet, the treatment efficacy in PDA has been limited because of the unique TMIE outline above. Due to the systemic collapse of the vasculature, chemotherapeutic agents such as gemcitabine, capecitabine, and 5-FU are surmised to be ineffective. While much effort is being put in to developing combination therapy to achieve the necessary toxicity, without a firm understanding of the biophysical mechanism behind the pathogenesis, the problem persists.

Provenzano et. al, recently proposed a unique insight on the problem. As mentioned above, the efficacy of chemotherapeutic treatment of endocrine pancreatic tumors is an important problem, attributable partly to the limited efficacy of therapeutic agents [2]. The authors propose the poor effectiveness of treatment is ascribed to the diminished transport of the drug into the tumor tissue. The central thesis of the paper is that alleviation of the interstitial fluid pressure (IFP) via enzymatic degradation of hyaluronic acid (HA) can improve the transport of chemotherapeutic agents into PDA stroma, and improve the effectiveness of chemotherapeutic treatment of PDA. They reason PEGPH20 degrades HA, relieves the vessels of IFP, and facilitates gemcitabine delivery which is confirmed in a murine model treated with a combined therapy of the chemotherapeutic gemcitabine and the HA ablating enzyme PEGPH20. The paper shows promising results.

The goal of this review is to provide an exhaustive critique of the merits and limitations of Provenzano et. al, highlight the controversy regarding the mechanism which results in elevated interstitial pressures, and suggest alternate mechanisms for the observed result. This review also reviews the transport mechanisms affecting solute concentrations in the PDA, and suggests improvements to the models and experimental methods used in the paper.

## **SUMMARY OF THE EXPERIMENTAL DATA**

### **Approach and General Methods**

In the paper, Provenzano et. al first investigate the cancer stroma and its environment with immunohistochemical methods [6]. The stainings show that the initial cancer lesions develop into a stroma with a dense matrix with high collagen content. Over time the relative concentration of collagen and glycosaminoglycans (GAG), especially HA, increases. Pancreatic stellate cells infiltrate

early on and remain active throughout the progression of the disease maintaining the matrix' growth.

To further understand the physical property of the tumor microenvironment (TMIE), the authors measure what they assume to be the interstitial fluid pressure (IFP) in autochthonous PDA and normal pancreata with a 25 gauge needle miniature piezoelectric pressure transducers (Millar Micro Tip pressure catheter). These *in vivo* measurements reveal that the pressure in normal pancreata is significantly lower (8-13mmHg) than that in PDA (75-130 mmHg), suggesting that the TMIE impedes convection and diffusion of small molecules into the tumor.

To investigate the relation between HA content and IFP, the authors first seed primary murine PDA cells in a three-dimensional lattice with different HA concentrations and implant them in immunodeficient mice. The experiment shows a HA content of at least 3mg/ml causes a doubled pressure baseline which leads to the assumption that a systemically administered enzyme such as PEGPH20 could ablate HA and lead to a facilitated delivery of molecules by decreasing the IFP. PEGPH20 is first tested on wild-type mice without causing noticeable changes to animal health or behavior. Then it is administered intravenously to KC and KPC mouse models with PDA. The pressure readings approach normal pancreatic levels 24h after treatment. In order to evaluate how the change in pressure affects the vascularity, the authors then evaluate blood vessel diameters, finding a significant change in total number of blood vessels of sizes of  $> 10\mu m$  as well as a shift to larger mean diameter in the distribution of CD31+ vessels. Moreover, about 75% of vessels in PDA have no lumen without PEGPH20 administration, compared to 29% of the vessel after treatment.

The functionality of the vasculature is evaluated with an intravital multiphoton laser scanning microscope. With labeled doxorubicin, the delivery of small molecules is probed. Vessels in normal pancreata show unhindered drug delivery throughout the organ. vessels in PDA are hard to find and appear collapsed; Doxorubicin penetration into the tumor is limited. After PEGPH20 administration blood vessels in PDA become discernible with 6.5-fold increase of fluorescence intensity from doxorubicin. From this observation, authors surmise that high IFP is the main cause of vascular collapse and thus main impediment for drug delivery.

In order to put this hypothesis to the test, Provenzano et al. administer the original preclinical dose of gemcitabine and PEGPH20 ("combination treatment") in a three weeks on, one week off, regime to KPC mice with PDA. This experimental group is compared to a cohort that was treated

with gemcitabine and a placebo in a randomized trial. Tumor size is assessed with high resolution ultrasound measurements and IFP is measured through the inserted Millar sensors. In mice treated with the combination treatment, IFP normalizes shortly after the drugs are administered. The IFP of gemcitabine and placebo treated mice remain high. These findings are also evident in tumor composition after necropsy. The extracted tumors are softer, and highly vascularized if the combination treatment was received. Placebo and gemcitabine treated animals show no change in tumor size after the first round of treatment while 83% of PEGPH20 and gemcitabine treated mice' tumors shrink after one treatment cycle and 100% of them after three cycles. The combined treatment causes the number of stromal PSC and active PSC in PDA to decrease. Collagen content is assumed to decrease due to the adverse effects on PSC. No effect on endothelial cell proliferation or apoptosis is noticed. The treatment has similar effects on existing metastases while the frequency of malignant ascites, metastases to liver, lungs, diaphragm and mesenteric lymph nodes decreases in the combined treatment. The overall survival rate increases by 83% after three months of treatment.

The absorption dynamics are modelled with the Kedem-Katchalsky equation that incorporates diffusive and convective transport. The pressure driven flow is assumed to follow Starling's hypothesis that osmotic pressures inside and outside a boundary are approximately equal and the PDA internal pressure is much higher than that in the blood vessels. Moreover, the osmotic reflection coefficient approaches zero for small molecules thus neglecting osmotic transport. While both small and large molecules can be transported by convection due to the leaky nature of tumor vessels, the high pressure in IFP causes negligible transport contributions by convection. Furthermore, since the total vascular area in PDA is small, diffusive transport is also very small. Upon administration of PEGPH20 the vessel area increases and the PDA internal pressure decreases causing an increase in both convective and diffusive transport into the tumor. The mathematical models of transport phenomena are discussed in more detail in improvements.

## **Strengths and Weaknesses**

The experimental approaches of Provenzano et al. [6] show the expertise of the authors in the field. They question the reliability of traditional cancer graft models and instead investigate autochthonous cancers in PDA specific mouse models. This allows them to incorporate the authentic cancer environment into their investigation and more specifically lead to the identification of HA

as a primary component of the PDA stroma. They understand that this environment is a major hurdle for existing treatments. By measuring the PDA internal pressure they draw the conclusion the dense ECM is likely prohibiting molecules to enter. The decision that in order to combat the high pressure readings targeting the ablation of HA through an enzymatic reaction is the key clinical insight of the paper. In the end, the authors are able to present promising results for the combination therapy in PDA.

There are several sections, however, that need further validation and experimental as well as theoretical work. As discussed later in the controversy section, the theoretical model for the transport mechanism is underdeveloped. This is partly due to the lack of a clear definition of what is meant by IFP; does it refer to the liquid phase of interstitium only? Or does it include viscoelastic, gel-phase of HA? A clear working mechanism that incorporates the change of IFP in a comprehensive physical model is missing.

The uncertainty around IFP is especially problematic, as the authors employ a non-standard pressure measurement tool by using the Millar pressure transducer. They fail to validate and confirm their IFP measurements with other measurement techniques. This is fatal as they may potentially disregard systemic measurement errors and cues to understand the physical background of drug delivery.

Moreover, concerning their functional analysis experiment, the use of doxorubicin needs to be explained or reconsidered. The principal agent of deployment in the latter murine study is gemcitabin, which has different chemical and molecular properties in the given TMIE. Wei et al. demonstrated that doxorubicin is positively charged at pH 7.0 while gemcitabin has a net neutral charge [7]. According to a study by Rotin et al., the median pH of normal, non-cancerous tissue is 7.5, while that of tumor is 7.0 [8]. Though a slightly lower pH is expected for highly negatively charged HA ECM, a pH under 6.0 is highly unlikely in biologically relevant tissues. Thus, assuming the net charge state of doxorubicin and gemcitabin is fundamentally different in PDA, the functional analysis of drug delivery with electrochemically distinct agent is questionable.

Finally, the authors may want to elaborate on their method for counting blood vessels in TMIE. The 3D nature of the samples can complicate light-based counting of vessels. Specifically, the authors need to elaborate on how they estimated number for sufficiently compressed vessels where none of the marker molecules could reach.

## CONTROVERSY

Provenzano et al. propose a biophysical model for the observed TMIE in PDA by assuming that the elevated IFP due to HA proliferation is enough to collapse the vessels. When  $P_{IFP} > P_{IVP}$ , the pressure gradient causes the vessels to collapse and limits diffusion and convection to the interstitia, impeding gemcitabine delivery. The author hypothesizes that PEGPH20 enzymatically degrades stromal HA matrix and lowers the IFP, thus relieving the vessels of high fluid pressure, favoring diffusion and convection. This mechanism is schematically illustrated in Fig. 7 of the main paper.

However, the proposed mechanism is controversial, if not incorrect, for two critical reasons: (1) As stated earlier, the authors proceed with the discussion without defining IFP. (2) The authors experimentally show at HA concentration of 3mg/ml, the measured IFP doubles. But, they do not explain how this result could be extrapolated to justify the ten-fold increase of measured IFP. In fact, they do not consider the charged nature of HA in the ECM, ending the discussion prematurely; As HA accumulates in the ECM, the repulsive electrostatic force is expected to generate a swelling pressure, which is not considered in their fluid mechanics model.

The proposed model is further undermined by the lack of discussion for the observed PEGPH20 delivery in PDA. Given how little is known of the PEGPH20 working mechanism, this may be understandable (with great foresight, Halozyme will eventually discontinue development of PEGPH20 in Nov. 2019 [9]) [10]. However, the authors need to elaborate on the reason as to why PEGPH20 is able to reach HA in the ECM while gemcitabine cannot.

Given this controversy, we analyze and validate their IFP measurement technique as well as their diffusion-convection model, and provide suggestions for improvements as needed. Also, a suggestion for repeating the functional analysis with gemcitabine is presented briefly as well.

## IMPROVEMENTS

## Functional Analysis with Gemcitabine

Though not directly related to the main controversy, performing functional analysis with gemcitabine, and not doxorubicin, will make Provenzano et al.'s argument that the antitumor agent is unable to reach PDA tissues in the murine combination therapy more consistent. This is especially important because at the pH of TMIE gemcitabine is expected to have a neutral net charge while doxorubicin is expected to have a net positive charge,  $z = +1$  [7]. Given a highly negatively charged ECM, the concentration of doxorubicin in the HA matrix would be much higher in quasi-Donnan equilibrium, leading to an exaggerated fluorescence intensity that may be significantly different for the signal from gemcitabine.

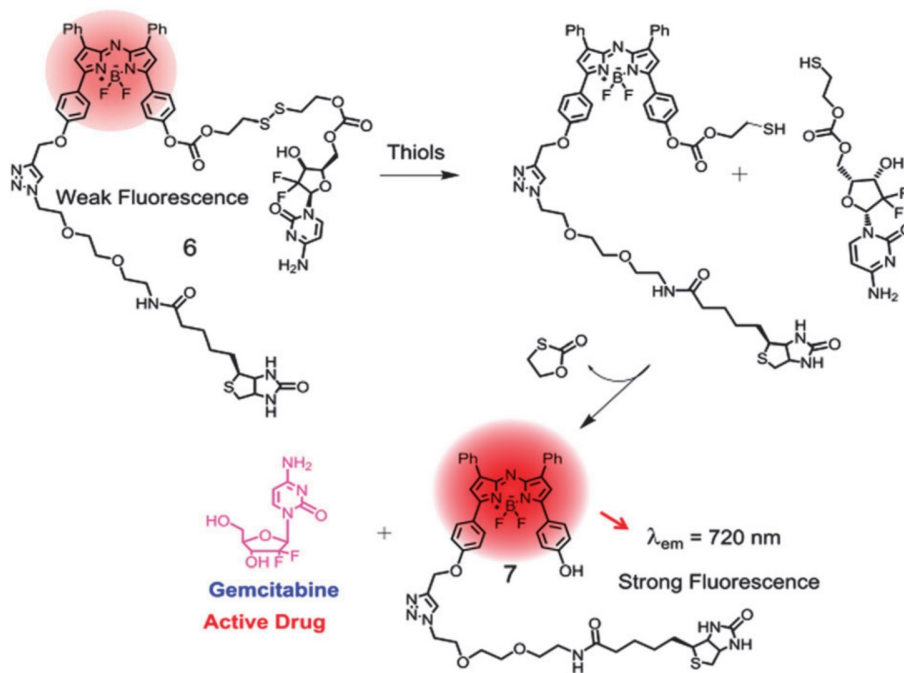


Figure 1: Scheme of drug release and increased fluorescence

The authors employed optical method to quantify doxorubicin in both normal and tumorous mouse pancreata. A similar optical technique can be performed with gemcitabine by conjugating it with a fluorophore. An in-vitro synthesis of such molecule is reported by Bhuniya et. al [11]. Their approach is to chemically synthesize a molecule composed of a biotin unit, which is a cancer-cell directing unit, a gemcitabine, and a theranostic prodrug. The synthetic scheme of the prodrug

component is outlined in Fig. 2. The mechanism of action for the complex is shown in Fig. 1. When the conjugated complex reaches the tumor cell, the intracellular thiol species cleaves the disulfide bridge, releasing active gemcitabine and enhancing fluorescence at 720 nm (near IR range). Bhuniya et al. further show that the cleaving reaction occurs only with biological thiol species, ensuring the reliability of the scheme. This can be used to monitor the gemcitabine penetration into the PDA tissues in real time similar to what Provenzano et al. did with doxorubicin.

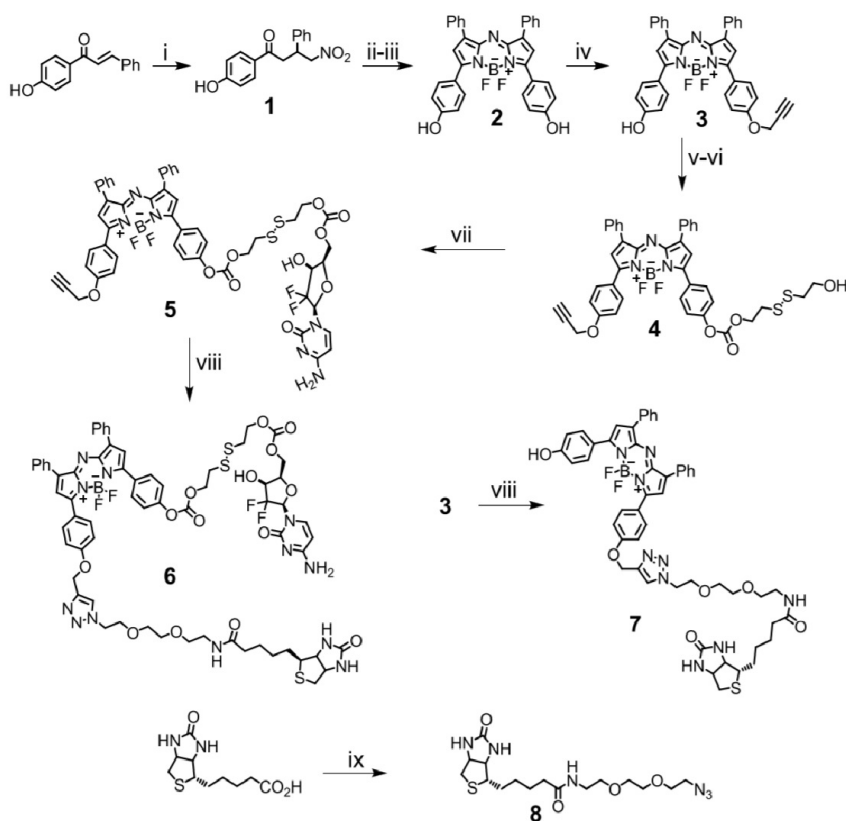


Figure 2: Prodrug synthesis: Reaction conditions: (i)  $\text{Et}_2\text{NH}$ ,  $\text{MeHO}_2$ ,  $\text{EtOH}$  reflux, 16h; (ii)  $\text{NH}_4\text{OAc}$  reflux, 24 h; (iii)  $\text{BF}_3$ ,  $\text{DIPEA}$ ,  $\text{DCM}$ , 12 h; (iv) propargyl bromide,  $\text{K}_2\text{CO}_3$ , acetone, reflux, 12 h; (v) mono-O-DMTr(4,4-dimethoxytrityl)-2-hydroxyethyl disulfide,  $\text{COCl}_2$ ,  $\text{DIPEA}$ ,  $\text{DCM}$ , 273–300 K, 12 h; (vi)  $\text{AcOH}$ ,  $\text{DCM}$ , 300 K, 24 h; (vii) 4-nitrophenyl chloroformate,  $\text{DIPEA}$ ,  $\text{DCM}$ , 273K–300K, 3 h then gemcitabine,  $\text{TEA}$ ,  $\text{DMF}$ , 300 K, 12 h; (viii) 8,  $\text{Na-ascorbate}$ ,  $\text{CuSO}_4$ ,  $\text{MeOH-H}_2\text{O}$ , 300K, 4 h; (ix) 2-(2-(2-azidoethoxy)ethoxy)ethanamine,  $\text{EDCI}$ ,  $\text{DMAP}$ ,  $\text{DMF}$ , 300K, 6 h.

## Interstitial Fluid Pressure Measurement Technique

Since IFP is at the base of the proposed working mechanism in the presented paper the reliability of the IFP measurement device has to be confirmed and investigated.

The authors measure the interstitial fluid pressure (IFP) by using a Millar Mikro-Tip pressure catheter transducer (SPR-1000) (Fig. 3 right). The device contains a piezoelectric sensor element that is side-mounted in a catheter. The sensor is based on a semiconductor crystal that generates a voltage output for a given pressure due to the piezoelectric effect. As a force is applied on the piezoelectric crystal, charges in the lattice are displaced perpendicular to the applied pressure direction causing a voltage with a linear pressure-voltage relationship. Before measurements, the MC is calibrated at 0, 25, and 100 mmHg and the calibration is confirmed after each study. It is put into the tumor by using a 25 gauge needle which is first inserted into the cancerous tissue, the probe is placed through the needle and then the needle is withdrawn.

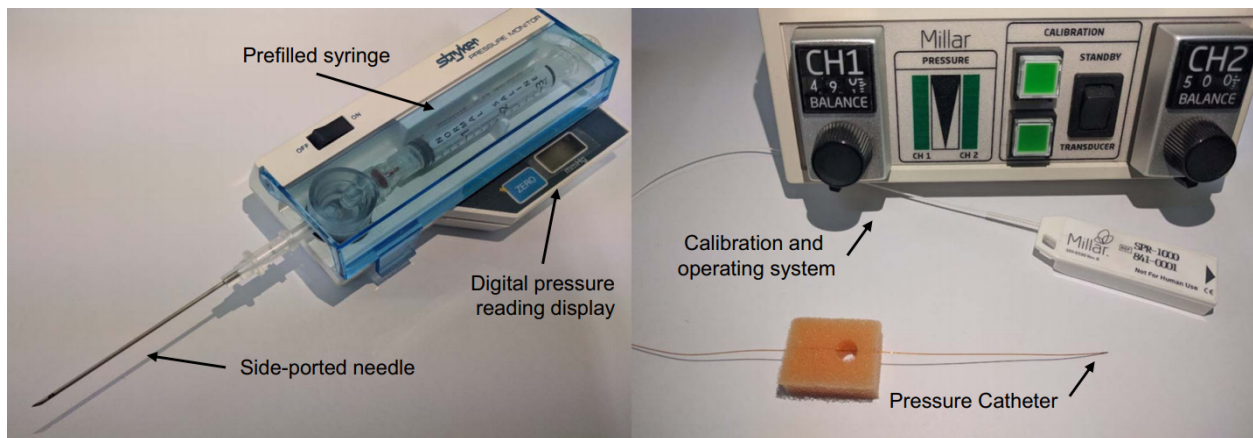


Figure 3: Pressure measurement methods. Left: Wick-in-needle technique. Right: Millar pressure catheter

The authors cite two references for using the Millar catheter (MC) and this approach. Ozerdem et al. [12] attempt to prove that this method is a means for reliable measurements of IFP in cancer tissues. The MC is compared with the wick in needle (WN) technique and then used to investigate IFP in melanoma grafts. The techniques yield average pressures of 9.2 and 9.0 cmH<sub>2</sub>O for the MC and the WN, respectively in skin graft tumors of two C57BL/6 mice after calibrating the sensor similarly to the current paper. No measuring artifacts were found in their present study. The other reference Provenzano et al. [6] cite, investigates the effect of HA degradation in TMIE through

the enzymes rHuPh20 and PEGPH20. In order to measure the IFP [13] uses a similar pressure transducer by Millar with a similar calibration method and measurement protocol. Elevated IFP of 40 and 34 mmHg in PC3 and DU145 tumors are found. After administration of PEGPH20 these values decrease by 84% and 15%, respectively.

Upon critical investigation of the MC itself, one must note that piezoelectric sensors measure the sum of all applied forces. When measuring the IFP the MC is therefore prone to solid pressure artifacts as it cannot differentiate between the fluid pressure and the solid pressure or other force sources. Unfortunately neither of the two presented references deliver enough evidence for the MC to dispel this concern and establish it as a reliable measurement method for IFP. [12] critically lacks statistical significance as the number of mice used is two. Additionally, the tumor is not only a melanoma, but also a graft which is not comparable to the autochthonous PDA environment in [6] and could yield other pressure sources. [13] has obvious similarities with [6], and would be a good source if it were able to show that the the MC works well in PDA and measures IFP reliably. However there is no citation, reasoning, or proof of the reliability of the MC in PDA as it is not compared to other established methods. Further research into the use of the MC also does not reveal previous application in cancer research or other validation of its measurements compared to other techniques in the field prior to 2012.

The WN technique represents the established standard for reliable IFP measurements in cancer research as of 2012 (Fig. 3 left). To measure the pressure, a thin (about 23 gauge) needle with a 2-3mm side hole about 4-5mm from the tip is used [14]. The needle is filled with several multifilamentous nylon threads of about 25um diameter. Polyethylene tubing connects the needle to a pressure transducer whose signal is amplified and digitally recorded. The needle and tubing are filled with saline solution. Zero pressure is set by placing the needle in a saline filled beaker and it is calibrated by placing it at different depths. As the needle is placed in a foreign medium, the local fluid is absorbed into the wick according to the local pressure which eliminates other pressure sources from interfering with the measurement.

The method was introduced in the above-described form by [14] which meticulously investigates the application of WN in different scenarios and concludes the technique to be a simple and rapid way to measure IFP in rodents. Other studies such as [15] and [16] have established WN as a reliable method to measure IFP in tumors and validated it against other methods such as the

micropipette technique.

In order to further support their claim, Provenzano et al. [6] should validate their measurements against the standard technique in the field and compare their IFP measurements with the MC with measurements using WN. If the device is not measuring a purely liquid portion of the pressure, then the paper must identify other alternative source of added pressure which may be defined as part of IFP or otherwise.

## Donnan Swelling of the Extracellular Matrix

As [6] fails to deliver a reason for the increased IFP in the PDA stroma we propose an explanation using a Donnan swelling model [17] that describes the swelling of the HA-hydrogel structure in the ECM. We model our system as a rectangular piece of ECM with some fixed charge  $\tilde{\rho}_m$  placed in a bath containing *NaCl* solution of physiological concentration  $c_0$ . Assuming electroneutrality within the gel,

$$\begin{aligned} \tilde{\rho}_m + \sum z_i F \tilde{c}_i &= 0 \\ -\frac{\tilde{\rho}_m}{F} &= \tilde{c}_{Na+} - \tilde{c}_{Cl-} + \tilde{c}_{H+} - \tilde{c}_{OH-} \end{aligned} \quad (1)$$

Here,  $z_i$  and  $\tilde{c}_i$  are the valance and concentration of species  $i$  inside the gel respectively., and  $F$  represents the Faraday constant. The solute concentration within the gel can be related to that outside the gel using the Boltzmann distribution:

$$\left(\frac{\tilde{c}_i}{c_{i,0}}\right)^{1/z_i} = \text{const.} \quad (2)$$

Thus, assuming that the concentration of sodium and chloride ions far exceed that of hydrogen and hydroxide ions, electroneutrality within the gel can be expressed as:

$$-\frac{\tilde{\rho}_m}{F} \approx \tilde{c}_{Na+} - \frac{c_0}{\tilde{c}_{Na+}} \quad (3)$$

The above equation can be represented as a quadratic equation:

$$\left(\frac{\tilde{c}_{Na+}}{c_0}\right)^2 + \frac{\tilde{\rho}_m}{F c_0} \left(\frac{\tilde{c}_{Na+}}{c_0}\right) - 1 = 0 \quad (4)$$

The solution to eq. 4 can be represented as:

$$\tilde{c}_{Na+} = -\frac{\tilde{\rho}_m}{2F} + \frac{c_0}{2} \sqrt{\left(\frac{\tilde{\rho}_m}{F c_0}\right)^2 + 4} \quad (5)$$

The total ionic strength within the gel can be represented as:

$$\tilde{c}_{tot} = \sum c_i \approx \tilde{c}_{Na+} + \tilde{c}_{Cl-} \quad (6)$$

If we assume that the gel has some fixed negative charge ( $\tilde{\rho}_m < 0$ ), we can determine from equation 5 that  $c^* = \tilde{c}_{Na+}/c_0 > 1$ . The ratio of the ionic strength inside to that outside the gel can be expressed as:

$$\frac{\tilde{c}_{tot}}{c_{tot,0}} = \frac{1}{2} \left( \frac{\tilde{c}_{Na+}}{c_0} + \frac{\tilde{c}_{Cl-}}{c_0} \right) = \frac{1}{2} \left( c^* + \frac{1}{c^*} \right) \quad (7)$$

The expression  $\frac{1}{2} \left( c^* + \frac{1}{c^*} \right) < 1$  only for  $-1 < c^* < 1$ . Since,  $c^* > 1$ , given a negatively charged gel, therefore, the total ionic strength inside the charged gel must be greater than the ionic strength outside in the bath. From the van't Hoff formula, osmotic pressure  $\Pi \sim cRT$  varies proportionally with the ionic strength  $c$ . Therefore, the osmotic pressure inside the gel is expected to be greater than that outside in the bath. This gradient in osmotic pressure between the gel and the bath causes osmotic movement of water across the semi-permeable gel membrane from the relatively low-concentration bath solution to the high-concentration gel matrix, resulting in Donnan swelling of the gel. This Donnan swelling allows for redistribution of ionic concentrations and for osmotic equilibrium to be achieved [17].

The ionic strength inside the gel depends heavily on the fixed charge density  $\tilde{\rho}_m$  of the matrix. ECM generally contains ionizable charged groups (such as sulphite and carboxyl groups) and is generally negatively charged at  $pH \approx 7$ . However, the charge density of the ECM can vary significantly with the acidity of the bathing solution. The fixed charge of the ECM can be modeled assuming that the matrix contains  $i$  ionizable charge groups  $A_i$  with dissociation constants  $K_i$ . Assuming electroneutrality, we can represent the fixed charge as:

$$\frac{\rho_m}{F} = \sum z_i c_i \quad (8)$$

The concentration of each ionizable charge group  $c_i$  can be represented in terms of its dissociation constant.



$$K_i = \frac{[A_i][H^+]}{[A_i H]} \quad (10)$$

Here,  $n_i$  represents the site concentration of charged groups of species  $i$ . For an acidic group, the charged group is  $A_i$  while for a basic group, the charged group is  $HA$ . Thus, the concentration of the charged group  $c_i$  is represented as:

$$\begin{aligned} c_i, a &= \frac{n_i K_i}{K_i + [H^+]}; \text{(acidic)} \\ c_i, b &= \frac{n_i [H^+]}{K_i + [H^+]}; \text{(basic)} \end{aligned} \quad (11)$$

Therefore, the total charge density of the ECM can be determined as:

$$\frac{\rho_m}{F} = \sum_i^{\text{acidic}} \frac{n_i z_i}{1 + 10^{(-pH+pK_i)}} + \sum_j^{\text{basic}} \frac{z_j n_j}{1 + 10^{(pH-pK_j)}} \quad (12)$$

Thus, the magnitude and sign of the fixed charge density of the gel depend on on the  $pH$  as well as the  $pK_i$  of the ionizable charged groups in the ECM. Given the complex desmoplastic nature of the PDA, the site concentration of ionizable groups  $n$  and the pH environment is likely to change over the course of the carcinoma. Titration of a section of the PDA ECM can help determine the isoelectric point and the fixed charge density of the gel as the PDA progresses, which in turn, can help predict the extent of Donnan swelling of the ECM.

We can estimate the osmotic pressure within the gel relative to that outside the gel using certain simplifying assumptions. Here, we assume that HA is the primary monomer imparting a net fixed charge to the ECM. Each monomer in the HA macromolecular structure contains an ionizable

carboxyl group, which dissociates with a  $pK \approx 3$  (each monomer also contains a amine group, but its dissociation can be expected to be small at physiological pH) [18]. The PDA stoma is also expected to be slightly acidic, with a  $pH \approx 6.5$  [19]. Thus, the fixed charge  $\rho_m$  of the gel can be determined for a range of HA concentrations using eq. 12. Given a fixed charge density, the ionic strength inside the gel can be determined using Equations 5 and 7. Here, we assume complete dissociation of the  $NaCl$  solution (i.e. ideal solution). Finally, the osmotic pressure  $\Delta P$  inside the gel, relative to the outside is determined using the van't Hoff equation.

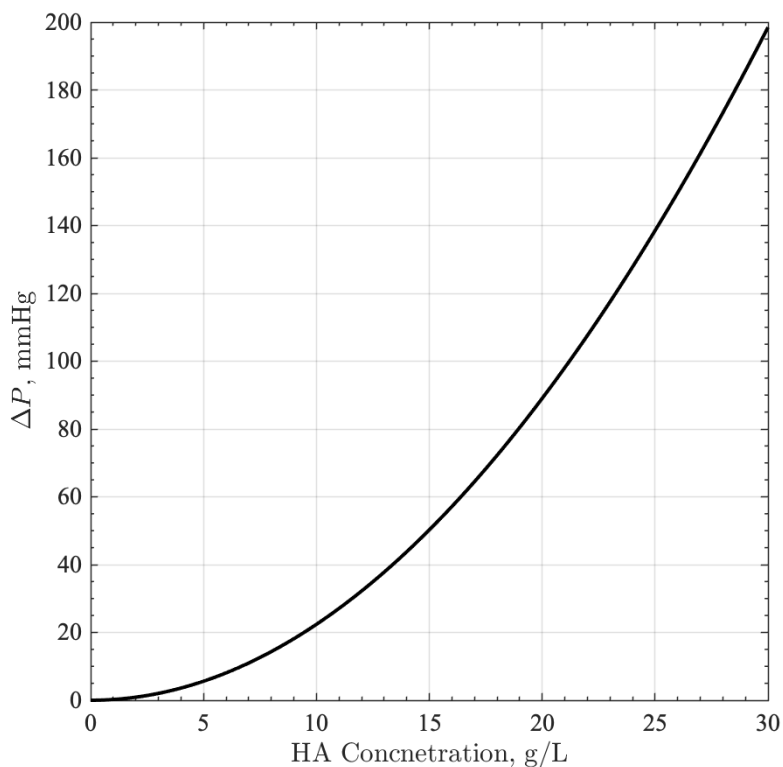


Figure 4: The variation of the relative osmotic pressure  $\Delta P$  inside the gel relative to the outside with HA concentration in the gel, assuming a physiological  $NaCl$  concentration of  $c_0 = 0.15M$

The variation of the relative osmotic pressure  $\Delta P$  inside the gel relative to the outside with HA concentration in the gel, assuming a physiological  $NaCl$  concentration of  $c_0 = 0.15M$  is shown in Fig. 4. The relative osmotic pressure  $\Delta P$  in the gel increases with increasing HA concentration, since the total negative fixed charge of the gel also increases with HA concentration, resulting in a larger discontinuity in ionic strengths inside and outside the gel. Provenzano et al. (2012)

report elevated IFPs on the range of  $\sim 100$  mm Hg within the PDA, which from Fig. 4, would be expected at a HA concentration of  $\sim 20g/L$ . Typical HA concentration within normal pancreatic tissue has been reported at  $\sim 29\mu g/g$  wet tissue ( $\approx 0.03g/L$ ), and  $\sim 388\mu g/g$  wet tissue ( $\approx 0.4g/L$ ) in PDA [20]. The elevated HA concentration in the PDA is thus not significant enough to cause an elevated IFP on the order of  $\sim 100$  mm Hg as reported in Provenzano et. al (2012). This suggests that the swelling of the gel is not the primary mechanism of elevated IFP, and that some other mechanism (such as solid stress) may be responsible for vascular collapse. Measurement of the HA concentration in the PDA inspected by Provenzano et al. (2012) and a comparison with the Donnan swelling pressure can better validate the hypothesis.

## Fluid Motion and Transport Mechanism

In order to validate the methodology and physical mechanisms employed by Provenzano et al., it is important to critically analyze both fluid motion and transport of solute (e.g. gemcitabine) around the vessel and tumor tissue. However, since the chemophysical conditions around the microvasculature and tumor bed are quite different, it is not easy to derive a single equation governing the entire system. Thus, for the plausible solution, we need separate the analysis into two distinct regimes; (A) the migration of fluid and solute from the intravascular compartment into the interstitial compartment across the semi-permeable vascular wall and (B) the diffusion and convection of the solute within the interstitial compartment characterized by dense porous ECM into the tumor tissue. Based on these theoretical approaches, we evaluated the hypothesis and argument conveyed by the article.

## Pressure Distribution and Solute Transport across a Semi-Permeable Vessel Wall

### Fluid Motion

The vessel in the tumor bed can be modeled as a cylinder of characteristic axial length  $L$  and radial length  $R$  with a thin, semi-permeable wall illustrated in Fig. 5. In the limit of steady, fully developed, incompressible, axisymmetric, viscous flow of a Newtonian fluid, and neglecting gravitational effects, the Navier-Stokes equation in the axial direction can be reduced to the Stokes equation in cylindrical coordinates.

$$0 = \frac{-\partial P}{\partial z} + \mu \frac{1}{r} \frac{\partial}{\partial r} r \frac{\partial v_z(r)}{\partial r} \quad (13)$$

Here,  $\mu$  is the dynamic viscosity of the fluid,  $\partial P/\partial z$  is the pressure gradient in the axial direction, and  $v_z(r, z)$  is the velocity in the z-direction. To obtain this equation, we also assume that the velocity  $v_r$  in the radial direction is small compared to that in the axial direction, since  $R/L \ll 1$ . Equation 13 describes Hagen-Poiseuille pipe flow (Fig. 5), and can be solved to determine the axial velocity  $v_z$ , assuming a no-slip boundary condition at the wall and a zero shear boundary condition at  $r = 0$ .

$$v_z(r, z) = \frac{R^2}{4\mu} \left( \frac{-\partial P}{\partial z} \right) \left( 1 - \frac{r^2}{R^2} \right) \quad (14)$$

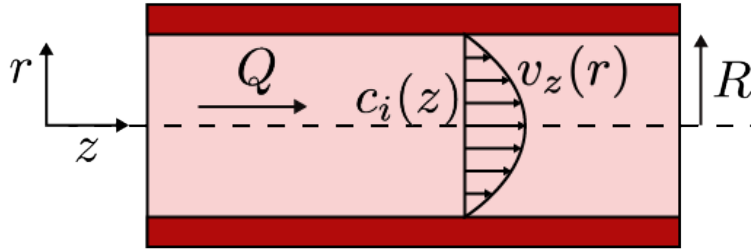


Figure 5: Fluid velocity profile of the Poiseuille flow inside the vessel with cylindrical coordinates

The volumetric flow rate  $Q$  can be determined from the area integral of the velocity as:

$$Q = \int_0^{2\pi} \int_0^R v_z(r) r dr d\theta = \frac{\pi R^4}{8\mu} \left( \frac{-\partial P}{\partial z} \right) \quad (15)$$

Thus, given a constant pressure gradient, the volumetric flow rate through the vessel is expected to vary as  $Q \sim R_i^4$ . This seems to support the hypothesis made by Provenzano et al. that vascular collapse inhibits transport, since a small decrease in vascular diameter can result in a significant decrease in flow rate and flux of the solute delivered to the site. However, note that the pressure gradient along the vessel can change, since flow rate  $Q$  varies along the z-direction because of the permeable wall. The variation of  $Q$  with respect to  $z$  can be expressed as

$$\frac{dQ}{dz} = -\frac{\pi R^4}{8\mu} \left( \frac{d^2 P}{dz^2} \right) \quad (16)$$

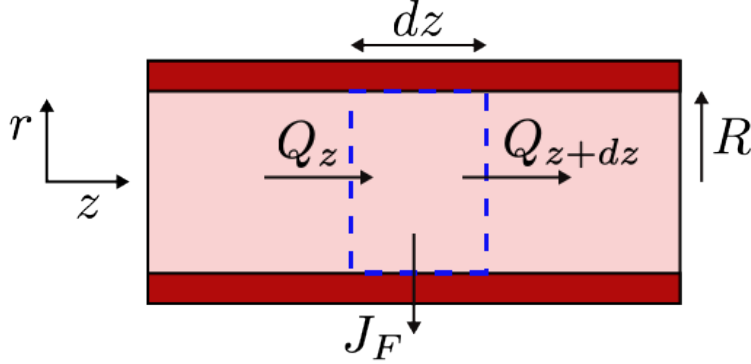


Figure 6: Differential control volume with volumetric flow rate  $Q_z$  in the axial direction, and fluid flux  $J_F$  exiting in the radial direction through the semi-permeable wall

Next, consider the mass conservation in the control volume of the vessel indicated in Fig. 6 with the blue line. Based on the Reynolds transport theorem, we can constitute an equation representing the relationship between the axial fluid volumetric flux  $Q_z$  and the pressure-driven fluid flux  $J_F$  across the membrane.

$$\left. \frac{dM}{dt} \right|_{sys} = \int_{CS(t)} \rho \vec{v} \cdot d\vec{A} = 0 \quad (17)$$

$$\int_{CS(t)} \rho \vec{v} \cdot d\vec{A} = (Q_{z+dz} - Q_z) + J_F = 0 \quad (18)$$

The fluid flux  $J_F$ , generated by the pressure gradient across the membrane can be determined by the classic Starling equation

$$J_F = L_p A \{ (P - P_i) - \sigma(\pi_v - \pi_i) \} \quad (19)$$

Here,  $L_p$  is the filtration coefficient of the vessel,  $A$  is the surface area of the vessel wall (which

is same as  $2\pi R dz$ ),  $P$  and  $P_i$  are vascular and interstitial hydrostatic pressures respectively, and  $\pi_v$  and  $\pi_i$  are vascular and interstitial colloid osmotic pressures respectively.  $\sigma$  represents the oncotic reflection coefficient. Since increased interstitial oncotic pressure in the adenocarcinoma cancels out the oncotic pressure inside the vessel, and the oncotic reflection coefficient is almost zero for micromolecules (Provenzano, 2012), the oncotic pressure term in the equation is negligible compared to the hydrostatic pressure term [6]. This simplified Starling equation can be substituted into the conservation equation we derived.

$$(Q_{z+dz} - Q_z) + 2\pi R L_P (P - P_i) dz = 0 \quad (20)$$

$$\frac{dQ}{dz} = -2\pi R L_P (P - P_i) \quad (21)$$

From Hagen-Poiseulle flow and mass conservation, we now have two equations representing the volumetric flow rate along the vessel. Since the differentiated flow rates with respect to  $z$  from both equations have to be identical, we can obtain the differential equation in terms of intravascular pressure (IVP).

$$\frac{dQ}{dz} = -\frac{\pi R^4}{8\mu} \left( \frac{d^2 P}{dz^2} \right) = -2\pi R L_P (P - P_i) \quad (22)$$

$$\frac{d^2 \mathcal{P}}{dz^2} = \lambda^2 \mathcal{P} \quad (23)$$

$$\mathcal{P} \equiv P - P_i, \quad \lambda \equiv \sqrt{\frac{16\mu L_P}{R^3}} \quad (24)$$

We defined relative pressure  $\mathcal{P}$  as a pressure difference between the IFP and IVP, and  $\lambda$  consisting of the fluid viscosity, filtration coefficient and radius of the vessel. To solve this second order linear ODE, we need two boundary conditions describing the invariable pressure value at certain points in the capillary vessel. First, assume that the IVP at  $z = 0$  and  $z = L$  is  $P_a$  and  $P_b$ , representing the location at the capillary near the terminal arterioles and venules, respectively. IFP,  $P_i$ , is considered to be constant and isotropic. Then the relative pressure  $\mathcal{P}$  at each point  $z = 0$  and  $z = L$  can be

expressed as

$$\mathcal{P}(z = 0) = P_a - P_i \quad (25)$$

$$\mathcal{P}(z = L) = P_b - P_i \quad (26)$$

By solving the second order ordinary differential equation with these boundary conditions, we can finally derive the relative pressure.

$$\mathcal{P} = \left[ \frac{(P_a - P_i) - (P_b - P_i)e^{\lambda L}}{1 - e^{2\lambda L}} \right] e^{\lambda z} - \left[ \frac{(P_a - P_i)e^{\lambda L} - (P_b - P_i)}{1 - e^{2\lambda L}} \right] e^{\lambda(L-z)} \quad (27)$$

Suitable quantitative data can be applied to this equation to evaluate the effect of increased pressure in stroma. The mean pressures value near the arterioles and venules are presumably 60 mmHg and 30 mmHg respectively, and the mean IFP is about 100 mmHg (Provenzano, 2012[6]). The filtration coefficient,  $L_p$  is about  $2.3\mu m/Pa \cdot s$  and the value of the dynamic viscosity is  $3.0 \times 10^{-3} Pa \cdot s$  (Williams, 1999[21] ; Wells, 1962[22]). Based on the numerical data of the vessel radius in the article, Provenzano et al., we estimated the pressure distribution along the vessel with a characteristic length  $L$  of  $100\mu m$ .

The IVP distribution in Fig. 7 clearly demonstrates that even though initial IFP is extremely high, the interior pressure can increase until it reaches the vicinity of the elevated external pressure. Due to the large fluid flux through the permeable vessel wall, the total fluid flux increases, and a reduced radius of the vessel wall facilitates the increment of the IVP. Because of this competitive counter pressure, increased IFP might not be the primary reason for the vascular collapse. Moreover, to establish the boundary condition, we previously assumed that interstitial pressure is constant and isotropic, meaning that it can affect the entire vessel uniformly. However, given that the actual IFP is likely driven by a solid-like hydrogel, assuming isotropic condition on entire vessel including both arterioles and venules might overestimate the actual effect of the IFP. Considering this IVP distribution, thus, the hypothesis suggested by the paper that increased IFP causes vessel collapse needs to be re-evaluated.

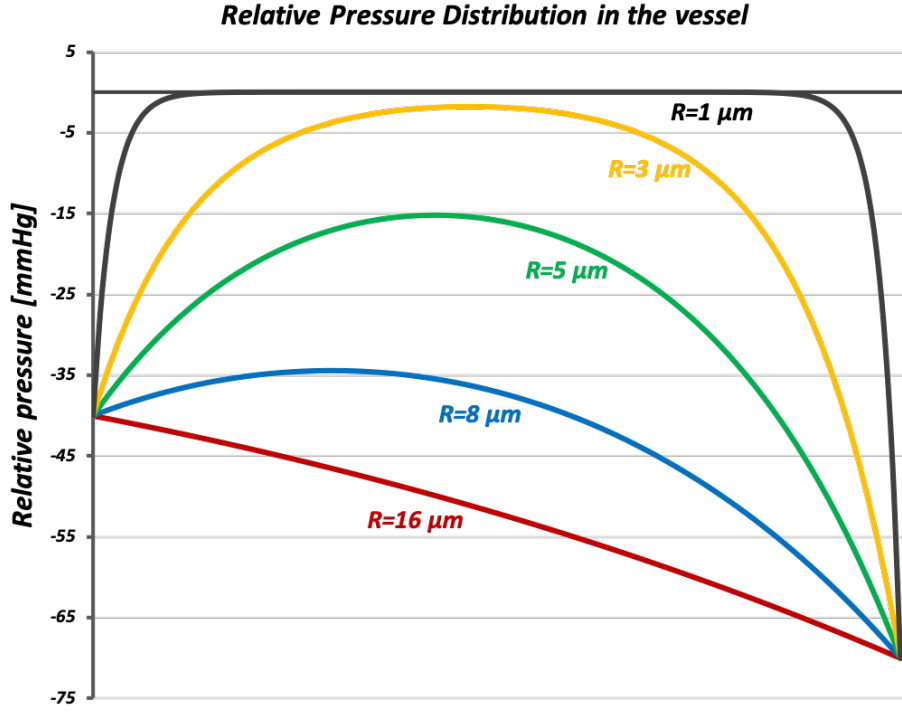


Figure 7: Relative vascular pressure distribution with respect to IFP. IVP approaches close to the elevated IFP when radius of the vessel decrease from  $16\mu m$  to  $8, 5, 3,$  and  $1\mu m$ .

## Molecular Transport

Analyzing the solute behavior around the vessel can help us not only to establish the primary driving force of transport across the vessel, but also to verify the previous hypothesis that Provenzano et al. suggested. To understand this transport mechanism, first we can consider the following transport equation governing the transport of any solute across the permeable vessel wall:

$$\frac{\partial c_v}{\partial t} = -\nabla \cdot \vec{N} + \dot{R} \quad (28)$$

Here,  $c_v$  represents the concentration of any solute in the vessel and  $\dot{R}$  is the rate of production of the solute. We will assume that this reaction term is negligible compared to the flux term.  $\vec{N}$  is the total flux of the solute, which can be represented by the Staverman-Kedem-Katchalsky equation ([23] and [24]) :

$$\vec{N} = P(c_v - c_i) \hat{r} + \frac{\vec{J}_F}{A} (1 - \sigma_F) \Delta c_{lm} \quad (29)$$

$$\Delta c_{lm} \equiv \frac{c_v - c_i}{\ln(c_v/c_i)} \approx \frac{1}{2}(c_v - c_i) \quad (30)$$

Here,  $P$  is the diffusive permeability,  $A$  is the surface area of the vessel,  $c_i$  represent the solute concentrations in the interstitial area,  $\sigma_F$  is solvent drag reflection coefficient, and  $\Delta c_{lm}$  is the log-mean concentration. To clarify the direction of the transport and calculate the vector operator, vector notation is additionally included. Combined with the fluid flux eq. (19) and van't Hoff osmotic pressure eq. (31), the solute flux eq (29) can be plugged into the conservation eq. (28).

$$\Delta\pi = \pi_v - \pi_i = RT\Delta c \quad (31)$$

$$\frac{\partial c_v}{\partial t} = -\nabla \cdot \left[ (c_v - c_i) \left( P + \frac{L_P}{2}(1 - \sigma_F)\mathcal{P} - \frac{L_P}{2}(1 - \sigma_F)\sigma RT\Delta c \right) \right] \hat{r} \quad (32)$$

Equation (31) is van't Hoff osmotic pressure equation.  $R$  is ideal gas constant and  $T$  is absolute temperature. Equation (32) contains all factors influencing the rate of the solute transport, diffusion and convection driven by hydrostatic and osmotic pressure. However, we do not need to consider every single term in this equation, if one of the driving forces are more dominant than the others. In fact, we can show that diffusion effect can be neglected unless the relative pressure is too small. If we compare the diffusive permeability  $P(\approx 6 \times 10^{-3} \mu m/s)$  [25] to the hydrostatic pressure term  $(L_P/2)(1 - \sigma_F)\mathcal{P}(\approx \mathcal{P} \cdot 2.8 \times 10^1 \mu m/s \cdot mmHg)$  [21] [26], we can numerically evaluate the relative effect of diffusion compared to convection. Thus, assuming  $Pe \gg 1$  across the vessel wall can be validated. This is also well-matched with the previous assumption proposed by the article. Rearranging the equation delivers

$$\frac{\partial c_v}{\partial t} = -\frac{L_P}{2}(1 - \sigma_F)[\mathcal{P} + 2\sigma RT(n - c_v)] \frac{\partial c_v}{\partial r} \quad (33)$$

$$n = c_v + c_i \approx c_i \quad (34)$$

Here, we assumed that the solute transport is only relevant in the radial direction. Also, the volume of the interstitial region is big enough to make  $c_i$  constant during the entire transport

process. We will use  $n$  to define the total concentration of the solutes. The eq. (33) is a first order non-linear PDE which can be further simplified if  $\partial c_v/\partial r \approx (n - c_v)/\delta$ , where  $\delta$  represents the characteristic distance of the solute transport across the permeable wall. Then the equation can be expressed as a first order non-linear ODE.

$$\frac{dc_v}{dt} = -\frac{LP}{2\delta}(1 - \sigma_F)[2\sigma RT(n - c_v)^2 + \mathcal{P}(n - c_v)] \quad (35)$$

Finally, we can derive the relative concentration equation of the solutes inside the vessel.

$$\frac{c_v}{n} = 1 - \left( \frac{Ae^{-Bt}}{1 + A - e^{-Bt}} \right) \quad (36)$$

$$A \equiv \frac{\mathcal{P}}{2\sigma RTn} < 1, \quad B \equiv -\mathcal{P} \frac{LP}{2\delta}(1 - \sigma_F) \quad (37)$$

To find the solution of this non-linear equation, we defined  $A$  as a non-dimensional value, which is smaller than 1, representing the dominant effect of the hydrostatic pressure compared to oncotic pressure. Next, to demonstrate the trend of the concentration variation, we used the following numerical values: Gas constant  $R = 0.062 \text{m}^3 \cdot \text{mmHg}/\text{K} \cdot \text{mol}$ ,  $T = 310\text{K}$ ,  $\sigma_F = 0.82$  (Wolf, 1987 [26]), characteristic length  $\delta = 1\mu\text{m}$ . Although we neglected the osmotic reflection coefficient  $\sigma$  in terms of the fluid motion, for now, we do not restrict the physical size of the molecules for oncotic convection and assumed  $\sigma \approx 0.5$  as a mean value. We varied the relative pressure  $\mathcal{P}$  from  $-20\text{mmHg}$  to  $-100\text{mmHg}$ . The initial relative concentration of the solute was set as 0 as a boundary condition.

The results are plotted in Fig. 8. The solute concentration reaches the equilibrium within a few microseconds even at the small relative pressure. This means oncotic pressure by the solute concentration difference is negligible unless we are focusing on the transport within the similar characteristic time scale. Thus, the assumption (i.e. neglecting the oncotic pressure) made by Provenzano et al. is reasonable considering the time scale. Another interesting point is that the rate of solute concentration is highly dependent on relative hydrostatic pressure. Note that after  $4\text{ms}$ , the relative concentration reaches 0.2 when  $\mathcal{P}$  is  $-20\text{mmHg}$ , whereas it is almost 0.9 when the pressure is  $-30\text{mmHg}$ . However, there is no such huge variation when the pressure increases from  $-30\text{mmHg}$  to  $-100\text{mmHg}$ . Thus, elevated IFP does not highly affect both the fluid motion and

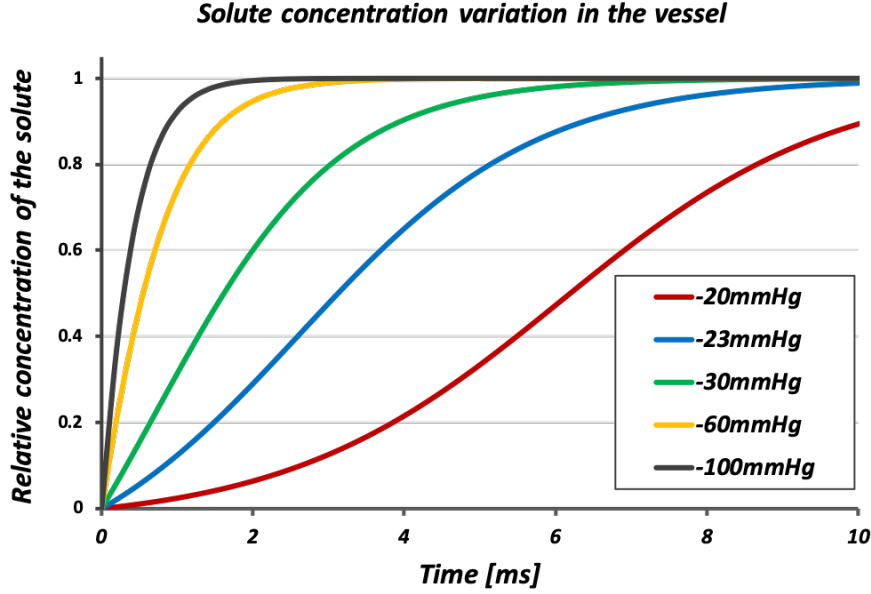


Figure 8: concentration ratio at the intravascular region. The rate of solute concentration increases when high IFP is applied on the vessel.

molecular transport, which consequently rebuts the article, emphasizing the significant influence of increased IFP on the vessel.

### Transport within the Interstitial Compartment

Next, we investigate the transport within the interstitium. The total solute flux in the ECM is given by:

$$N_i = -D_i \nabla c_i + V c_i + \frac{|z_i|}{z_i} c_i u_i E \quad (38)$$

Here,  $D_i$  is the diffusivity of the solute,  $V$  represents the velocity field of the fluid in which the solute is dispersed,  $z_i$  and  $u_i$  are the valence and the electrical mobility of the solute, and  $E$  is the electric field.

### Molecular Transport

In the absence of an applied electric field, the transport within the ECM is governed by diffusion and convection. We will first examine the diffusive flux  $-D_i \nabla c_i$  of the solute within the ECM. Provenzano et al. hypothesize that a denser ECM inhibits the diffusion of solute into the tumor

tissue. This claim can be verified by modeling the ECM as a porous medium and predicting the effect of ECM density on the diffusivity  $D_i$  of the solute. A porous medium is characterized by a porosity  $\omega$  and a tortuosity  $\tau$ . Porosity  $\omega$  is defined as the ratio of the fluid volume to the total volume of the porous medium, and is a measure of the void fraction of the material. Tortuosity  $\tau$  is a measure of the connectivity of the porous network, and is defined as the ratio of flow path length to the straight distance between the ends of the flow path. The diffusivity of a solute of finite size in a porous medium differs from its diffusivity in a fluid. An effective diffusivity  $\mathcal{D}$  can be considered for porous media, and is commonly defined as [27]:

$$\mathcal{D} = \frac{\omega}{\tau} D_0 \quad (39)$$

Here,  $D_0$  represents the molecular diffusivity of the solute, which can be determined from the random walk model of molecular diffusion, and is given by the Einstein-Smoluchovski relation  $D_0 = kT/6\pi\mu R$ , where  $k$  is the Boltzmann constant,  $T$  is the temperature and  $R$  is the characteristic radius of the molecule. The effective diffusivity,  $\mathcal{D}$  thus, depends on the ratio of porosity and tortuosity  $\omega/\tau$  of the porous medium. The relation can be further simplified using the empirical Bruggeman relation  $\tau = 1/\sqrt{\omega}$  [27]. Thus, eq. 39 can be expressed as:

$$\mathcal{D} = \omega^{3/2} \frac{kT}{6\pi\mu R} \quad (40)$$

Therefore, given constant temperature, the effective diffusivity  $\mathcal{D}$  varies as  $\mathcal{D} \sim \omega^{3/2}$  with the porosity of the medium. This model supports the hypothesis made by Provenzano et. al that denser ECM can reduce diffusive flux  $-\mathcal{D}\nabla c_i$  into the tumor tissue, assuming that the porosity of the medium decreases with increasing ECM density. Measurements of the porosity or effective diffusivity of the ECM in PDA were not made by Provenzano et. al and thus, this model was not experimentally verified. However, it must be noted that the above model may elucidate general trends, but is limited in its ability to account for pore geometry and non-linear phenomena, such as, the diffusion of charged molecules [27].

Pore diameter  $w$  can also have a significant effect on the effective diffusivity of the solute. In particular, the diffusive regime can be determined using the Knudsen number  $Kn = \lambda/w$ , where  $\lambda$  is the mean free path of the molecule in a space with characteristic length  $w$ . The diffusivity  $D_i$  of

a molecule can be expected to vary with the ratio of the mean square displacement  $\langle \Delta x^2 \rangle$  and the inter-collision time  $t_c$ .

$$D_i \sim \frac{\langle \Delta x^2 \rangle}{t_c} \quad (41)$$

Given a constant temperature  $T$ , the kinetic energy of the molecule, and thus its velocity, will be constant, and the average inter-collision time  $t_c = \lambda/v$  will also be a constant. This, the diffusivity can be represented as:

$$D_i \sim \lambda v \quad (42)$$

For a small pore diameter,  $Kn \ll 1$ , and the effective diffusivity of the molecule is reduced due to a smaller mean free path available to the molecule. The Knudsen diffusivity  $D_{Kn}$  can thus be defined as  $D_{Kn} \sim wv$  and will be lower than the molecular diffusivity  $D_0 \sim \lambda v$ . In the intermediate regime, the effective diffusivity  $\mathcal{D}$  can be determined from the Bosanquet relation [27]:

$$\mathcal{D} = \left( \frac{1}{D_0} + \frac{1}{D_{Kn}} \right)^{-1} \quad (43)$$

Thus, the pore diameter  $w$  and the porosity  $\omega$  are important factors which govern the diffusive flux within the ECM. A systematic study of the effect of these factors on the effective diffusivity of solute within the PDA ECM would better inform the hypothesis made by Provenzano et al.

## Fluid Motion

Next, we will examine the convective flux  $Vc_i$  of the molecule within the ECM. Fluid flow in the ECM can be described by the Stokes equation, assuming steady, low Reynolds number, incompressible flow. In the limit of a porous media, the solution to the Stokes equation can be described by Darcy's law [27]:

$$v_x = \frac{\kappa}{\mu\omega} \left( \frac{-\partial p}{\partial x} \right) \quad (44)$$

Here,  $\kappa$  is the anisotropic permeability,  $\omega$  represents the porosity of the medium and  $p$  is the pressure within the ECM. A lack of pressure gradients within the ECM due to homogeneously high interstitial pressure would result in little fluid flow within the porous ECM, resulting in little advection of the solute. Thus, this model would support the hypothesis made by Provenzano et al., given a homogenous pressure distribution in the ECM. The homogeneity of the pressure in the interstitial compartment, however, was not experimentally verified but could be by measuring interstitial pressure along a range of points within the ECM.

Finally, we consider the diffusion-advection of the solute through the porous ECM. Assuming a 1D system with flow and diffusion in the x-direction, the advection-diffusion equation for a solute is represented as:

$$\frac{\partial c_i}{\partial t} + \left(\frac{\partial v_x}{\partial x}\right)c_i = \mathcal{D} \frac{\partial^2 c_i}{\partial x^2} \quad (45)$$

Here,  $\mathcal{D}$  represents the effective diffusivity of the solute in the porous medium, and  $v_x$  is the fluid velocity field determined from Darcy's law. Equation 45 can be non-dimensionalized as follows:

$$\begin{aligned} \left(\frac{c_0}{\tau_c}\right) \frac{\partial c^*}{\partial t^*} + \left(\frac{c_0 \mathcal{V}}{L}\right) \frac{\partial v_x^*}{\partial x^*} c^* &= \left(\frac{c_0 \mathcal{D}}{L^2}\right) \frac{\partial^2 c^*}{\partial x^{*2}} \\ \left(\frac{L^2}{\tau_c \mathcal{D}}\right) \frac{\partial c^*}{\partial t^*} + \left(\frac{\mathcal{V} L}{\mathcal{D}}\right) \frac{\partial v_x^*}{\partial x^*} c^* &= \frac{\partial^2 c^*}{\partial x^{*2}} \\ c^* &\equiv \frac{c_i}{c_0}, t^* \equiv \frac{t}{\tau_c} \\ v_x^* &\equiv \frac{v_x}{\mathcal{V}}, x^* \equiv \frac{x}{L} \end{aligned} \quad (46)$$

$\mathcal{V}$  is the characteristic velocity,  $\tau_c$  is the characteristic time of diffusion,  $c_0$  is the initial solute concentration and  $L$  is the characteristic length of transport. The expression  $\frac{\mathcal{V} L}{\mathcal{D}}$  is defined as the Peclet number  $Pe$  and can be described as the ratio of characteristic diffusion time to characteristic convection time. Using Darcy's law (eq. 44), the characteristic velocity can be expressed as  $\mathcal{V} \sim \kappa \Delta P / \mu \omega L^2$ , where  $\Delta P$  is the pressure differential within the ECM. Substituting this expression into that for the Peclet number, we obtain:

$$Pe = \frac{\kappa}{\mu \omega \mathcal{D}} \left(\frac{\Delta P}{L}\right) \quad (47)$$

Convection will only dominate the flow when  $Pe \gg 1$ . However, assuming no pressure gradient  $\Delta P/L$  within the ECM due to homogenous, elevated IFP, the Peclet number is likely to be small  $Pe \ll 1 \sim 0$ . Thus, we can expect the transport of the solute within the ECM to be completely driven by diffusion. The diffusion-advection equation can be solved numerically. Here, we solve the 2D diffusion-advection transport problem in a rectangular porous medium of characteristic length  $L = 1mm$  in COMSOL. The top boundary of the porous medium ( $y = 0$ ) has a constant flux boundary condition which can be determined with the Staverman-Kedem-Katchalsky equation. The time-dependence of the total solute concentration at a line half-way through the matrix ( $y = 0.5L$ ) for different porosities is shown in Fig. 9 for diffusion-dominated ( $Pe \ll 1$ ) transport. As expected, the total solute concentration is observed to decrease with decreasing porosity, which is in agreement with Provenzano et al.

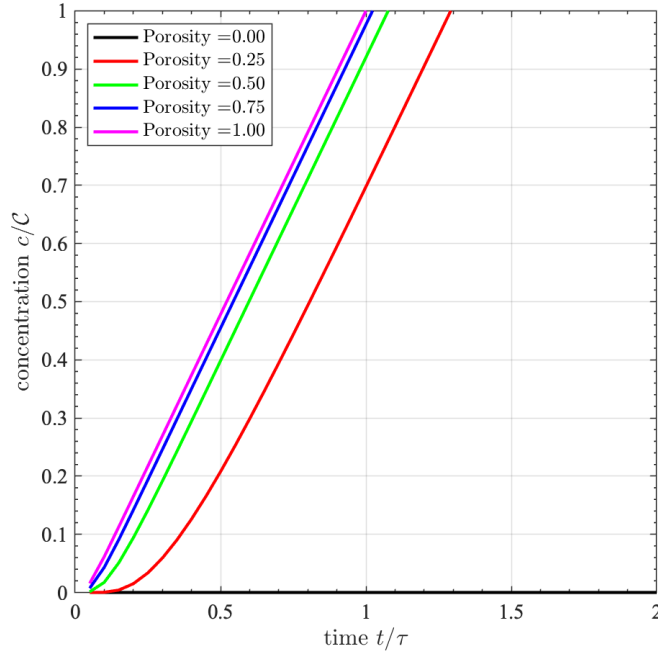
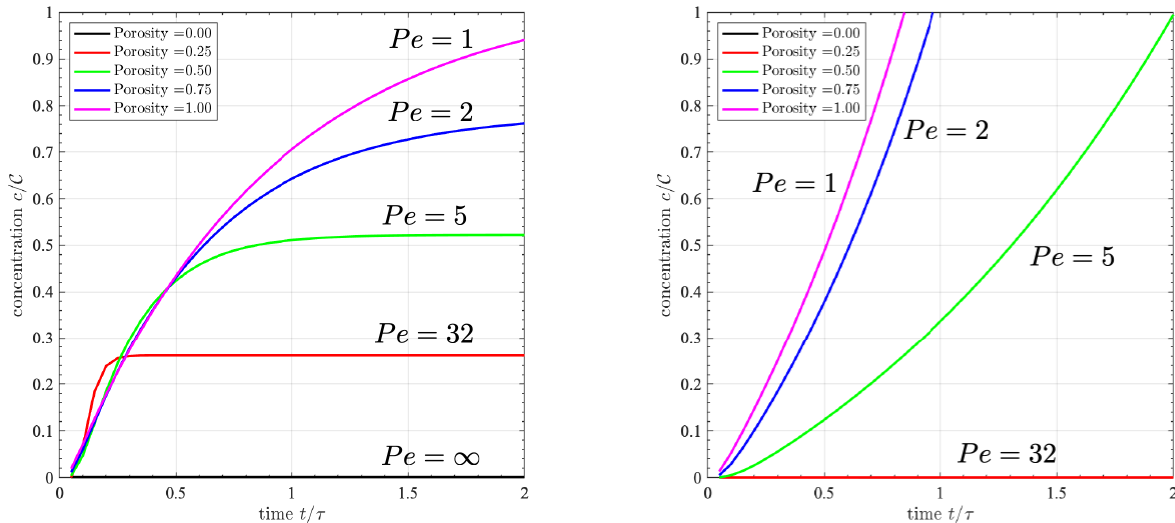


Figure 9: The time-variation of the total solute concentration at a line half-way through the matrix ( $y = 0.5L$ ) of characteristic length  $L$  for different porosities, for diffusion-dominated ( $Pe \ll 1$ ) transport. Here, the characteristic time is defined as  $\tau = L^2/\mathcal{D}$ , and  $\mathcal{C}$  is defined as the solute concentration at  $y = 0.5L$  at porosity  $\omega = 1$  and time  $t = \tau$ .  $\mathcal{D}$  is the effective diffusivity of the solute in the porous medium. As expected, the total solute concentration is observed to decrease with decreasing porosity, which is in agreement with Provenzano et. al's hypothesis.

In the presence of a pressure gradient, convection plays an important role in the transport

of the solute within the porous ECM. The diffusion-advection equation was solved in COMSOL in the presence of pressure gradients within the ECM. The time-dependence of the total solute concentration at a line half-way through the matrix ( $y = 0.5L$ ) for different porosities is shown in Fig. 10, both for diffusion against and diffusion with the flow.



(a) Diffusion of Solute in flow direction. With increasing porosity, the total solute concentration at  $y = 0.5L$  is observed increase. In each case, a steady state is achieved where the incoming fluid flux at  $y = 0.5L$  is balanced by the outgoing advective flux at that location.

(b) Diffusion of Solute against flow direction. With increasing porosity, the total solute concentration at  $y = 0.5L$  is observed increase. However, solute is not transported to  $y = 0.5L$  for porosity  $\omega \leq 0.25$  since convection dominates and inhibits any diffusion away from the inlet boundary.

Figure 10: The time-dependence of the total solute concentration at a line half-way through the matrix ( $y = 0.5L$ ) for different porosities in the presence of a pressure gradient.

Therefore, to comprehensively describe the transport of gemcitabine in the porous ECM, it is important to validate the assumptions of homogenous elevated interstitial pressures, and to examine the effect of porosity and pore diameter of the ECM on the effective diffusivity of the solute. The hypothesis of limited transport by convection and diffusion within the ECM made by Provenzano et al. would be better supported by systematic examination of these assumptions.

## RECOMMENDATIONS

### **Functional Analysis of Blood Vessels**

The authors performed functional analysis with doxorubicin only, which has a different charge property than gemcitabine. Conducting the experiment again with gemcitabine will improve the overall consistency of the paper since the combination therapy is performed with gemcitabine, not doxorubicin. To perform a functional analysis with gemcitabine, the relevant anti-tumor agent, we propose the authors utilize theranostic prodrug to create fluorescent gemcitabine as done by Sankarprasad et al. The complex fluoresces in the right tumor environment at near-IR range and can be quantified with similar optical method [11].

### **Measuring Interstitial Fluid Pressure**

The IFP was measured by Provenzano et al. with a MC. As explained above, the measurements using the MC are insufficient as the transducer itself has not been validated in PDA and it remains unclear whether it yields reliable results. In the paper the authors are unable to confirm whether the measurements contain solid stress artifacts which is a concern since piezoelectric sensors are inherently known to measure the sum of applied forces. It is therefore necessary that the measurements are repeated to investigate and support the proposed physical model. As the WN technique reliably measures IFP and has been the standard in the field for many years, experiments comparing measurements of WN with measurements of MC in the same KC and KPC mouse models in vivo are needed to confirm the reliability and clinical impact of these findings.

The Hingorani group actually followed up on this in 2016. DuFort et al. [28] compare WN and the MC in several tissues and discover discrepancies between the pressure readings of WN and MC. They claim that WN measures free-fluid pressure while the MC includes additional gel-fluid pressure and propose that better understanding the physiology that leads to increased gel-fluid pressure could yield better clinical outcome. They can however still not provide a physical explanation behind the elevated pressure readings.

## Donnan Swelling Pressure

Our calculations of the Donnan swelling pressure demonstrated that HA might not be the primary determinant for elevating IFP, considering the plausible concentration of the HA around the PDA. To consolidate this argument, we suggest measurement of HA concentration in the interstitium around the PDA. There are several methods based on chemical reactions to quantify the HA, such as carbazole assay using sulfuric acid and carbazole or turbidity assay reacting cetyltrimethylammonium bromide with the HA to form an insoluble complex [29]. In addition to chemical detection, we can also estimate the concentration without affecting the sample using near infrared spectroscopy with real-time monitoring [30]. These empirical approaches including theoretical analysis (Donnan equilibrium and van't Hoff equation) can help us to derive the Donnan swelling pressure and determine the relative influence of the HA on the total IFP.

## Intravenous Pressure Measurement

Provenzano et al. proposed that the vascular collapse in PDA is caused by extremely elevated IFP. However, considering the relative pressure derived from Starlings and Hagen-Poiseuille flow equations, IVP also increases against the IFP, which eventually cancels out the influence of the external pressure. Thus, additional experiments measuring the IVP need to be performed to clarify the effect of the IFP. First, it is necessary to estimate the velocity of the fluid in the capillary using cross correlation technique. This computerized method measures the velocity of red blood cells inside the vessel using two photometric windows. Together with the capillary microscopy and fluorescent dye (e.g. Indocyanine green for RBC), we can calculate the fluid velocity and approximate the cross sectional area of the vessel. Then we can find the volumetric flow rate, which gives us the magnitude of IVP based on eq. (21). Alternatively, we can consider the measurement of IVP using a resistance null-balance feedback system, which computes the wave pressure of the cannulated capillary and head/tail cannulation values to get the average value of the IVP [31]. A third option would be the use of gravimetric techniques to measure the IVP. Kietys et al. measured the pressure of pancreatic capillary attached vertically to a force transducer [32]. By controlling the arterial flow rate using a blood flow probe, they measured the venous pressure, which equals to capillary pressure in the isogravimetric state. By using these proposed experiments, the validity

of the hypothesis of vascular collapse driven by hydrostatic pressure can be assessed and we even other possible mechanisms can be explored.

### **Transport in the Extracellular Matrix**

Transport within the porous ECM is governed by diffusion and convection. The effective diffusivity of the solute in the ECM varies significantly with the porosity and pore size of the medium. Experimental measurement of the effective diffusivity of the ECM in PDA, and its comparison with normal tissue, can better support the authors' hypothesis. Examples of commonly used methods to determine diffusivity in biological systems include using a diffusion cell, or using optical fluorescence methods. Fluorescent microscopic imaging can also be used to determine the size and distribution of the pores within the ECM. Similarly, the assumption that IFP is homogeneous within the ECM can be experimentally verified by probing the pressure at multiple locations within the ECM to generate a pressure distribution.

### **References**

- [1] J. Kleeff, M. Korc, M. Apte, C. La Vecchia, C. D. Johnson, A. V. Biankin, R. E. Neale, M. Tempero, D. A. Tuveson, R. H. Hruban, *et al.*, "Pancreatic cancer," *Nature reviews Disease primers*, vol. 2, p. 16 022, 2016.
- [2] A. McGuigan, P. Kelly, R. C. Turkington, C. Jones, H. G. Coleman, and R. S. McCain, "Pancreatic cancer: A review of clinical diagnosis, epidemiology, treatment and outcomes," *World journal of gastroenterology*, vol. 24, no. 43, p. 4846, 2018.
- [3] A. S. Quante, C. Ming, M. Rottmann, J. Engel, S. Boeck, V. Heinemann, C. B. Westphalen, and K. Strauch, "Projections of cancer incidence and cancer-related deaths in germany by 2020 and 2030," *Cancer medicine*, vol. 5, no. 9, pp. 2649–2656, 2016.
- [4] C. E. Clark, S. R. Hingorani, R. Mick, C. Combs, D. A. Tuveson, and R. H. Vonderheide, "Dynamics of the immune reaction to pancreatic cancer from inception to invasion," *Cancer research*, vol. 67, no. 19, pp. 9518–9527, 2007.
- [5] U. M. Mahajan, E. Langhoff, E. Goni, E. Costello, W. Greenhalf, C. Halloran, S. Ormanns, S. Kruger, S. Boeck, S. Ribback, *et al.*, "Immune cell and stromal signature associated with progression-free survival of patients with resected pancreatic ductal adenocarcinoma," *Gastroenterology*, vol. 155, no. 5, pp. 1625–1639, 2018.
- [6] P. P. Provenzano, C. Cuevas, A. E. Chang, V. K. Goel, D. D. V. Hoff, and S. R. Hingorani, "Enzymatic targeting of the stroma ablates physical barriers to treatment of pancreatic ductal adenocarcinoma," *Cancer Cell*, vol. 21, no. 3, pp. 418–429, 2012.

- [7] J. Wang, X. Xing, X. Fang, C. Zhou, F. Huang, Z. Wu, J. Lou, and W. Liang, "Cationic amphiphilic drugs self-assemble to the core-shell interface of pegylated phospholipid micelles and stabilize micellar structure," *Philosophical Transactions of the Royal Society A: Mathematical, Physical and Engineering Sciences*, vol. 371, no. 2000, p. 20120309, 2013.
- [8] I. F. Tannock and D. Rotin, "Acid pH in tumors and its potential for therapeutic exploitation," *Cancer research*, vol. 49, no. 16, pp. 4373–4384, 1989.
- [9] *Halozyme announces halo-301 phase 3 study fails to meet primary endpoint*, <https://www.halozyme.com/investors/news-releases/news-release-details/2019/Halozyme-Announces-HALO-301-Phase-3-Study-Fails-To-Meet-Primary-Endpoint/default.aspx>, Accessed: 2019-11-30.
- [10] H. M. Shepard, "Breaching the castle walls: Hyaluronan depletion as a therapeutic approach to cancer therapy," *Frontiers in oncology*, vol. 5, p. 192, 2015.
- [11] S. Bhuniya, M. H. Lee, H. M. Jeon, J. H. Han, J. H. Lee, N. Park, S. Maiti, C. Kang, and J. S. Kim, "A fluorescence off-on reporter for real time monitoring of gemcitabine delivery to the cancer cells," *Chemical Communications*, vol. 49, no. 64, pp. 7141–7143, 2013.
- [12] U. Ozerdem and A. R. Hargens, "A simple method for measuring interstitial fluid pressure in cancer tissues," *Microvascular Research*, vol. 70, no. 1, pp. 116–120, 2005.
- [13] C. B. Thompson, H. M. Shepard, P. M. O'Connor, S. Kadhim, P. Jiang, R. J. Osgood, L. H. Bookbinder, X. Li, B. J. Sugarman, R. J. Connor, S. Nadjombati, and G. I. Frost, "Enzymatic depletion of tumor hyaluronan induces antitumor responses in preclinical animal models," *Molecular Cancer Therapeutics*, vol. 9, no. 11, pp. 3052–3064, 2010.
- [14] H. Fadnes, R. Reed, and K. Aukland, "Interstitial fluid pressure in rats measured with a modified wick technique," *Microvascular Research*, vol. 14, no. 1, pp. 27–36, 1977.
- [15] H. Wiig, R. K. Reed, and K. Aukland, "Measurement of interstitial fluid pressure in dogs: Evaluation of methods," *American Journal of Physiology-Heart and Circulatory Physiology*, vol. 253, no. 2, H283–H290, 1987.
- [16] Y. Boucher and R. K. Jain, "Microvascular pressure is the principal driving force for interstitial hypertension in solid tumors: Implications for vascular collapse," *Cancer Research*, vol. 52, no. 18, pp. 5110–5114, 1992.
- [17] H. Li, T. Y. Ng, Y. K. Yew, and K. Y. Lam, "Modeling and simulation of the swelling behavior of pH-stimulus-responsive hydrogels," *Biomacromolecules*, vol. 6, no. 1, pp. 109–120, 2005.
- [18] "Hyaluronan: Its nature, distribution, functions and turnover," *Journal of Internal Medicine*, vol. 242, no. 1, pp. 27–33, 1997.
- [19] C. W. Kimbrough, A. Khanal, M. Zeiderman, B. R. Khanal, N. C. Burton, K. M. Mcmasters, S. Vickers, and E. William, "Probes in vivo," vol. 21, no. 20, pp. 4576–4585, 2016.
- [20] A. D. Theocharis, M. E. Tsara, N. Papageorgacopoulou, D. D. Karavias, and D. A. Theocharis, "Pancreatic carcinoma is characterized by elevated content of hyaluronan and chondroitin sulfate with altered disaccharide composition," *Biochimica et Biophysica Acta - Molecular Basis of Disease*, vol. 1502, no. 2, pp. 201–206, 2000.
- [21] D. A. Williams, "Network Assessment of Capillary Hydraulic Conductivity after Abrupt Changes in Fluid Shear Stress," *Microvascular Research*, vol. 57, no. 2, pp. 107–117, 1999.
- [22] J. Roe E. Wells and E. W. Merrill, "Influence of Flow Properties of Blood upon Viscosity-Hematocrit relationships," *The Journal of Clinical Investigation*, vol. 41, no. 8, pp. 1591–1598, 1962.

- [23] O. Kedem and A. Katchalsky, “A Physical Interpretation of the Phenomenological Coefficients of Membrane Permeability,” *The Journal of General Physiology*, vol. 45, no. 1, pp. 143–179, 1961.
- [24] A. Staverman, “Non-Equilibrium Thermodynamics of Membrane Processes,” *Transactions of the Faraday Society*, vol. 48, pp. 176–185, 1952.
- [25] F. Yuan, M. Leunig, D. A. Berk, and R. K. Jain, “Microvascular permeability of albumin, vascular surface area, and vascular volume measured in human adenocarcinoma ls174t using dorsal chamber in scid mice,” *Microvascular Research*, vol. 45, no. 3, pp. 269–289, 1993.
- [26] P. D. W. Matthew B. Wolf and D. R. C. S. II, “Integral-mass balance method for determination of solvent drag reflection coefficient,” *American Journal of Physiology*, vol. 253, no. 1, H194–H204, 1987.
- [27] D. M. Tartakovsky and M. Dentz, “Diffusion in Porous Media: Phenomena and Mechanisms,” *Transport in Porous Media*, vol. 130, no. 1, pp. 105–127, 2019.
- [28] C. C. DuFort, K. E. DelGiorno, M. A. Carlson, R. J. Osgood, C. Zhao, Z. Huang, C. B. Thompson, R. J. Connor, C. D. Thanos, J. S. Brockenbrough, P. P. Provenzano, G. I. Frost, H. M. Shepard, and S. R. Hingorani, “Interstitial pressure in pancreatic ductal adenocarcinoma is dominated by a gel-fluid phase,” *Biophysical Journal*, vol. 110, no. 9, pp. 2106–2119, 2016.
- [29] J.-M. Song, J.-H. Im, J.-H. Kang, and D.-J. Kang, “A simple method for hyaluronic acid quantification in culture broth,” *Carbohydrate Polymers*, vol. 78, no. 3, pp. 633–634, 2009.
- [30] Q. Dong, H. Zang, L. Zang, A. Liu, Y. Shi, and H. Zhang, “Rapid determination of hyaluronic acid concentration in fermentation broth with near-infrared spectroscopy,” *Journal of Innovative Optical Health Sciences*, vol. 7, pp. 1450012.1–1450012.7, 2014.
- [31] A. C. Shore, “Capillaroscopy and the measurement of capillary pressure,” *British Journal of Clinical Pharmacology*, vol. 50, no. 6, pp. 501–513, 2000.
- [32] P. Kvietyš, J. McLendon, G. Bulkley, M. Perry, and D. N. Granger, “Pancreatic circulation intrinsic regulation,” *American Journal of Physiology*, vol. 242, no. 6, G596–G602, 1982.